Research Article

Vibration Response Characteristics of the Cross Tunnel Structure

Jinxing Lai,[1,2] Kaiyun Wang,[2] Junling Qiu,[2] Fangyuan Niu,[2] Junbao Wang,[3] and Jianxun Chen[1,2]

[1]*Shaanxi Provincial Major Laboratory for Highway Bridge & Tunnel, Chang'an University, Xi'an 710064, China*
[2]*School of Highway, Chang'an University, Xi'an 710064, China*
[3]*School of Civil Engineering, Xi'an University of Architecture and Technology, Xi'an 710055, China*

Correspondence should be addressed to Jinxing Lai; 373159626@qq.com and Jianxun Chen; chenjx1969@chd.edu.cn

It is well known that the tunnel structure will lose its function under the long-term repeated function of the vibration effect. A prime example is the Xi'an cross tunnel structure (CTS) of Metro Line 2 and the Yongningmen tunnel, where the vibration response of the tunnel vehicle load and metro train load to the structure of shield tunnel was analyzed by applying the three-dimensional (3D) dynamic finite element model. The effect of the train running was simulated by applying the time-history curves of vibration force of the track induced by wheel axles, using the fitted formulas for vehicle and train vibration load. The characteristics and the spreading rules of vibration response of metro tunnel structure were researched from the perspectives of acceleration, velocity, displacement, and stress. It was found that vehicle load only affects the metro tunnel within 14 m from the centre, and the influence decreases gradually from vault to spandrel, haunch, and springing. The high-speed driving effect of the train can be divided into the close period, the rising period, the stable period, the declining period, and the leaving period. The stress at haunch should be carefully considered. The research results presented for this case study provide theoretical support for the safety of vibration response of Metro Line 2 structure.

1. Introduction

Generally, the initial damage to the shield tunnel is caused by construction near the crossing tunnel as the repeated vibration rapidly promotes tunnel disasters. In particular, the most damage occurs during the later construction planning of the city. Many complicated construction projects have not been considered during the early construction, which can influence the exiting tunnels. For example, traversing with underneath passing or oblique crossing and close-range parallel passing of existing tunnels on the tunnel that is under construction successively appears, causing initial damage to the tunnel inevitably. The initial damage is accumulated during operation, which can ultimately result in the decrease of structure resistance and loss of function due to the long-term repeated function of the vibration effect.

Consequently, a number of research studies have been conducted. The response of buildings to train loading at different speeds was evaluated and then compared with the allowable vibration limits by Balendra et al. [1]. Using 2D and 3D models, Soliman et al. [2] discussed and studied the mutual influence of construction near parallel tunnels. Yamaguchi et al. [3] described the characteristics of influence from the thrust of a succeeding tunnel to a preceding tunnel and the analytical expression of the mechanism of ground behaviour during the construction of closely running tunnels. Koziol and Mares [4] analyzed the theoretical response of a solid to fast moving trains by using models related to real situations: a load moving in a tunnel and a load moving on the surface of the tunnel. Shi et al. [5] investigated the settlement behaviours of a metro tunnel during metro operation based on a nonlinear vibration model of vehicle track. Zhong et al. [6] constructed a measurement system based on the CompactRIO system and the LabVIEW platform to measure the ground-borne vibration induced by the subway, while Lai et al. [7] established a wireless sensor network (WSN)
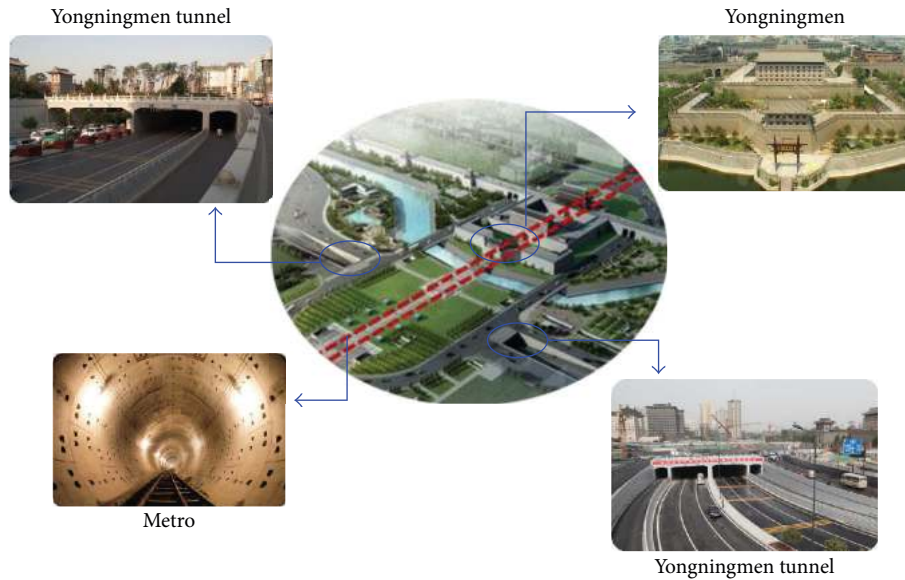
FIGURE 1: The location of the Yongningmen tunnel and Metro Line 2.

to monitor the effect of the blast-induced vibration on the structure of an existing tunnel.

However, most of the aforementioned studies concentrate on the dynamic response analysis under metro train vibrating load, whereas few studies have conducted a dynamic analysis under a highway tunnel of vehicle vibrating load. The research conducted on the combined interaction of the above two conditions is virtually nonexistent. Moreover, the differences in geological environment and the vehicle model do not allow the study results to be directly applied to the Xi'an metro. Therefore, with the numerical model based on Midas-GTS software, vibrating and mechanical response rules were proposed and supported by CTS of the Xi'an Yongningmen tunnel and Metro Line 2 shield tunnel.

2. Description of the Studied Tunnel

Yongningmen, commonly known as South Gate, is located at the central southern gate of the Ming Dynasty City Wall in Xi'an. The construction of the gate started in the early Sui Dynasty (AD 582), making it the oldest gate in Xi'an. Yongningmen has been included on the tentative list of World Cultural Heritage sites, along with the Ming and Qing Dynasties City Wall in China. The Yongningmen tunnel, a case study in this paper, is located near the Yongningmen gate, so it is imperative to evaluate the vibration response in this tunnel. The Yongningmen tunnel engineering starts at Zhenxing Road, continuing until the front door of the local Electric Power Co., Ltd., Shaanxi Province. The total length is 867 m, with a tunnel net length of 236 m, a width of 36.4 m, and a depth of 9.2 m. The Yongningmen tunnel is designed to be a bidirectional, six-lane tunnel; the route runs from east to west, and it opened to traffic in June 2014. As shown in Figure 1, the Yongningmen tunnel is at a right angle crossing relationship with Metro Line 2,

which began operation in September 2011. The Yongningmen tunnel includes 13 reinforced concrete cast-in-place slabs, of which the H6 and H8 slabs are located above shield tunnel of Yongningmen—the Bell Tower section of Metro Line 2. The slabs are only 2 m away from the shield tunnel vault, representing the shortest distance recorded of a relevant construction in China. To guarantee the safety of metro operation, grouting has been used to modify the soil property between the cover plate and the outer edge of the shield to improve the soil compactness and crack resistance. During operation of the tunnel, the propagation of vibration induced by the passage of vehicles inevitably resulted in long-term interference for the peripheral environment, in particular, Metro Line 2, which is only 2 m away from the Yongningmen tunnel. It will have a more prominent influence on the tunnel structure with the additional vibrations induced by the running trains.

The vibration responses were analyzed based on the numerical model in this paper, and the model should be reasonable and applicable. The method for the calibration of the FE model shown in Figure 2 is adopted. The whole model, including the parameters of viscous boundaries, was calibrated by comparing the numerical simulation results and the data registers measured under independent action of metro train (Condition 1). Then, the calculated results and those of field tests under Condition 2 were compared, and some conclusions were put forward.

3. Numerical Calculations

According to the typical geological materials for this section of Metro Line 2 in Xi'an, the soil is of a homogeneous medium, and the weighted average of the parameters of the soil property is taken as the calculation parameters. The properties of the soil layers are shown in Table 1.

TABLE 1: Properties of soil layers [32].

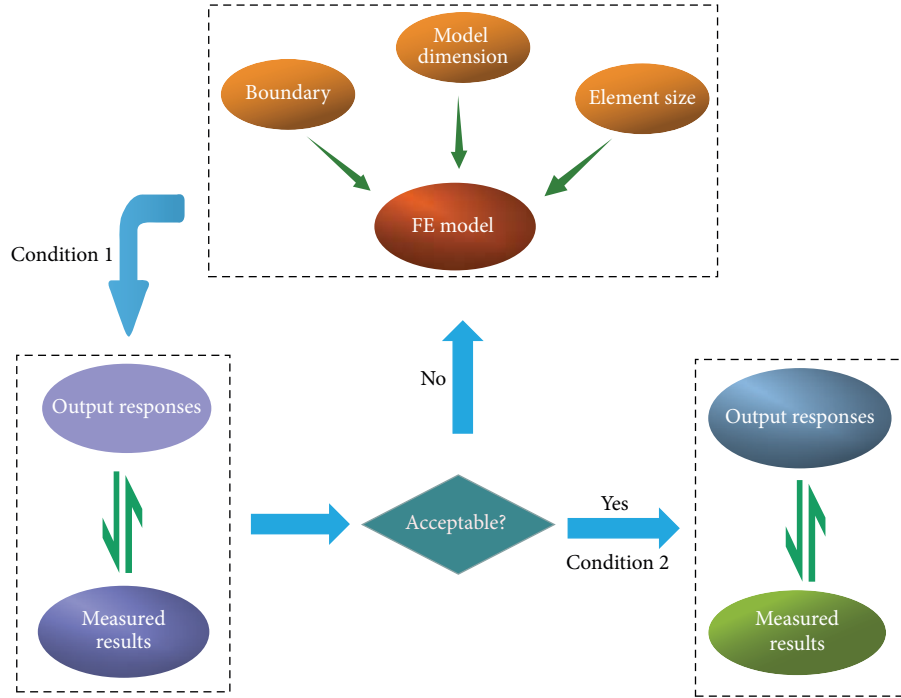| Soil layers	Natural unit weight (kN/m³)	Saturated unit weight (kN/m³)	Dynamic Poisson ratio	Cohesion (kPa)	Friction angle (degree)	Dynamic elastic modulus (MPa)	Shear wave velocity (m/s)
Plain fill	17.7	17.9	0.22	12.0	10.0	28.0	185
New loess	18.0	20.1	0.20	17.0	10.0	33.0	200
Improved soil	22.1	22.1	0.20	56.3	45.2	180.8	250
Old loess	20.5	20.9	0.25	30.0	26.0	46	230
Silty clay	20.5	20.9	0.30	32.0	24.0	75	235

FIGURE 2: Flow diagram for the calibration of the FE model.

The 3D model was established to study the dynamic response characteristics of shield tunnel structure. The distance L between model boundary and vibration source should be greater than the maximum half wavelength of the medium [8]:

$$L_{\min} = \frac{C_{\max}}{2f_{\min}}, \tag{1}$$

where C and f are the shear wave velocity and frequency. The minimum distance between model boundary and vibration source $L_{\min} = 11.90$ m, with $C_{\max} = 250$ m/s the maximum shear wave velocity. Therefore, the following model was selected to meet the accuracy of the solution. The model length is 48 m in horizontal direction; alone Metro Line 2 is 100 m. The bottom boundary of the model is 30 m below the ground level, and the upper surface of model is the free face of the ground level. A greater model is not used because of the long computation times involved. The geotechnical profile of the model is shown in Figure 3.

Considering the symmetrical model, the regular hexahedron elements were obtained by expanding 2D model to 3D model in Midas-GTS software. In order to accurately capture the volatility effect, the size of the finite elements should be smaller than the 1/6 times minimum wavelength corresponding to different soil layers [8]:

$$l_{\max} = \frac{C_i}{6f_{\max}}. \tag{2}$$

These results of the maximum element length of different soil layers $l_{\max}$ are 1.03 m, 1.11 m, 1.39 m, 1.28 m, and 1.31 m, respectively. In order to obtain the ideal element size, the peak values (positive and negative) of four key points under the conditions that element sizes $l = 0.5$ m, $l = 0.6$ m, $l = 0.8$ m, and $l = 1$ m were compared in Figure 4. Point A, on the vault, point B, on the spandrel, point C, on the haunch, and point D, on the springing of the tunnel, were selected as key points. The velocities with the element size of $l = 0.8$ m and $l = 1$ m are more close than that of $l = 0.5$ m and $l = 0.6$ m
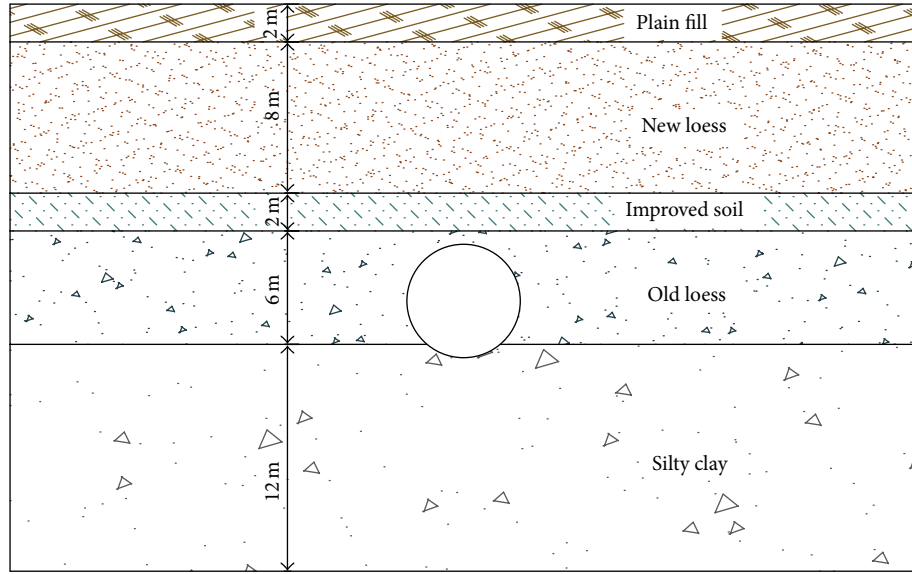
FIGURE 3: Geotechnical profile of the problem.

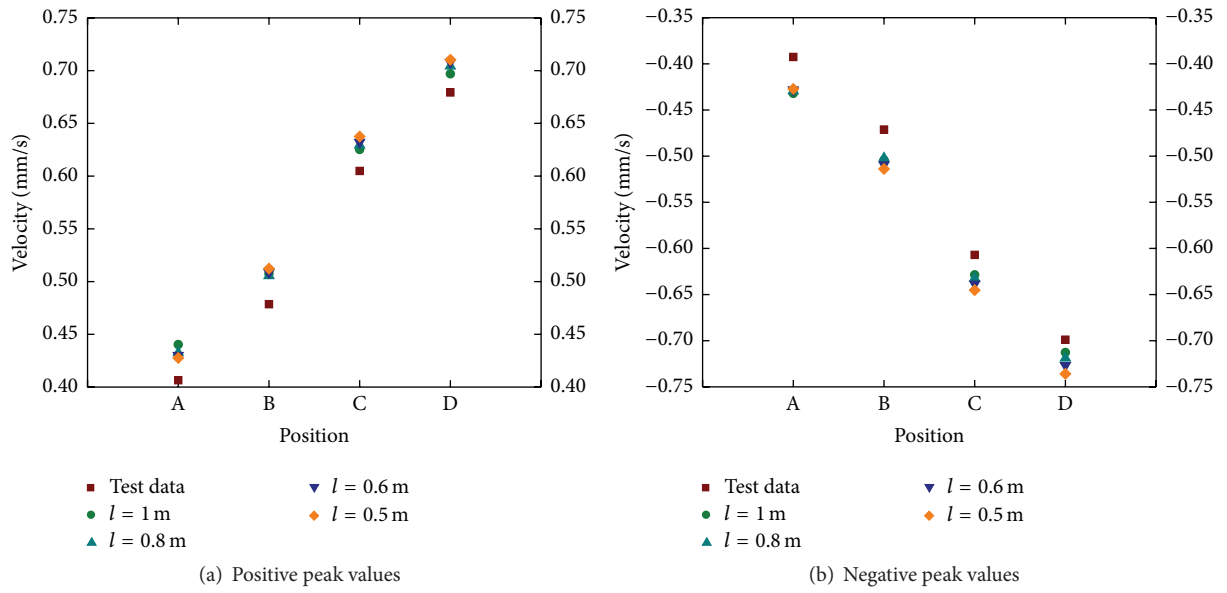(a) Positive peak values

(b) Negative peak values

FIGURE 4: Vibration velocities under different element sizes.

to those registers measured. The element length $l = 1$ m was recommended in this model for ease of analysis.

Free vibration analysis should be conducted to obtain inherent dynamic characteristics of model structure before time-history analysis. According to the literatures [8–10], the elastic boundaries were employed in the free vibration analysis and surface spring was created. The vertical coefficient of spring stiffness is calculated by

$$k_v = k_{v0} \cdot \left(\frac{B_v}{30} \right)^{-3/4} \tag{3}$$

and the horizontal coefficient of spring stiffness is

$$k_h = k_{h0} \cdot \left(\frac{B_h}{30} \right)^{-3/4}, \tag{4}$$

where $k_{v0} = (1/30) \cdot E_0 = k_{h0}$, $B_v = \sqrt{A_v}$, $B_h = \sqrt{A_h}$, A_v and A_h are calculation model area in vertical direction and horizontal direction, respectively, and E_0 is elastic coefficient of the foundation.

Because the reflection of the wave in the truncated boundary will produce large errors, viscous boundaries were

TABLE 2: Boundary parameters.

Soil layers	Coefficients of spring stiffness			Viscous parameters	
	K_x (kN/m^3)	K_y (kN/m^3)	K_z (kN/m^3)	C_{pi} (kN·s/m)	C_{si} (kN·s/m)
Plain fill	19980	26310	/	830	497
New loess	15214	18076	/	968	559
Improved soil	58591	77156	/	1834	981
Old loess	16221	22169	/	1014	585
Silty clay	20857	27486	12402	1268	768

TABLE 3: Results of free vibration analysis.

Mode number	1	2	3	4	5	6	7	8	9	10
Frequency (Hz)	2.04	2.10	2.26	2.36	2.60	2.65	2.67	2.88	3.42	3.53
Angular frequency (rad/s)	12.82	13.20	14.20	14.85	16.31	16.63	16.80	18.08	21.46	22.17

set during time-history analysis in Midas-GTS [8–10]. The damping constants of P-wave C_{pi} can be calculated by

$$C_{pi} = A_i \rho_i \sqrt{\frac{\lambda + 2G}{\rho_i}} \qquad (5)$$

and the damping constants of S-wave C_{si} can be calculated by

$$C_{si} = A_i \rho_i \sqrt{\frac{G}{\rho_i}}, \qquad (6)$$

where A_i is the boundary area; λ is the first lame constant, $\lambda = \nu E/(1 + \nu)(1 - 2\nu)$; G is shear modulus of elasticity, $G = E/2(1+\nu)$; ρ is the density of the material; E is elastic modulus; ν is Poisson ratio. The boundary parameters and results of free vibration analysis are depicted in Tables 2 and 3, respectively.

Generally, Rayleigh damping is used as a dynamic damping of systems in dynamic analyses. The damping matrix is proportional to the mass and stiffness matrices [11–13], and the expression is as follows:

$$[C] = \alpha [M] + \beta [K], \qquad (7)$$

where $[M]$, $[C]$, and $[K]$ are the mass matrix, damping matrix, and stiffness matrix of the system, respectively, and they are combined with the mass matrix, damping matrix, and stiffness matrix of all units together. The proportional damping constants α and β and the damping ratio should satisfy the following relationship:

$$\xi_k = \frac{\alpha}{2\omega_k} + \frac{\beta \omega_k}{2} \quad (k = 1, 2, \dots, n), \qquad (8)$$

where ξ_k is the damping ratio; ω_k is the inherent frequency; α and β are the proportional damping constants. According to the literatures [9, 14, 15], the damping ratio is assumed to be a constant value that $\xi = \xi_i = \xi_j = 0.05$ within the frequency

range (ω_i, ω_j). The free vibration equation of the system can be used to calculate the inherent frequency of ω_i and ω_j. Then,

$$\alpha = \frac{2\omega_i \omega_j}{\omega_i + \omega_j} \xi, \qquad (9)$$
$$\beta = \frac{2}{\omega_i + \omega_j} \xi.$$

Using the predominant frequency of participation mass $\omega_i = 12.82$ rad/s, $\omega_j = 13.20$ rad/s, the damping ratio $\xi = 0.05$, and based on (9), the value of Rayleigh damping is then determined as

$$[C] = 0.6504 [M] + 0.0038 [K]. \qquad (10)$$

4. Dynamic Load

4.1. Vehicle Load. The dynamic response of the moving load acting on the foundation is obvious only when it approaches the wave velocity of the foundation surface or the wave velocity of the internal modes of the foundation. However, the wave velocities of the highway structure surface and the internal modes are far higher than the speed of the vehicles. Therefore, the effect of vehicle speed on the dynamic response of the highway structure can be ignored in the case of full evenness of the pavement. In fact, the highway pavement may not be fully level, and the evenness of the pavement becomes increasingly worse with the increase of service time. When vehicles run on the bumpy pavement, vibrations are generated, thus creating additional dynamic load beyond the static load, which is the crucial difference between static and dynamic stress of highway structure.

For the convenience of dynamic analysis on the tunnel structure, supposing the vehicle is still on the road during vibration, the load vibration formula of the wheels [16, 17] to the road can be

$$F = k (y - h \sin \omega t), \qquad (11)$$
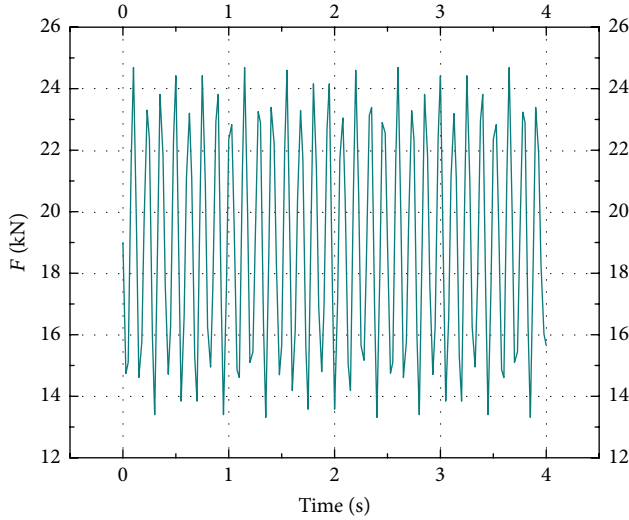
$$\omega = \frac{2\pi v}{\lambda}, \qquad (12)$$

FIGURE 5: Vibrating load versus time curve.

TABLE 4: Geometric parameters for UK railway engineering.

Control conditions	Wavelength (m)	Versine (mm)
	50.00	16.000
Driving comfort ①	20.00	9.000
	10.00	5.000
Dynamic additional	5.00	2.500
load to the road ②	2.00	0.600
	1.00	0.300
Corrugation ③	0.50	0.100
	0.05	0.005

FIGURE 6: Vibrating load versus time curve.

where k is tire stiffness, y is unsprung vertical displacement, h is amplitude of pavement roughness, ω is excitation frequency of pavement, v is running speed, and λ is wavelength of uneven pavement.

It can be observed from formula (11) that when vehicles are travelling on the rough pavement, the dynamic load of wheels to pavement changes with the time and evenness. The excitation curve of vehicle load in the first 4 s is shown in Figure 5.

4.2. Train Load. The train load has posed a complicated problem due to the factors involved, such as train axle load, suspension system, running speed, track structure, and track regularity [18–21]. The metro train load refers to the moving line load including random elements and constant elements. The main factors that affect the trains vibration load are wheel-rail interaction and dynamic effect. The irregular track and wheel-rail contact surface, weight of eccentric wheel, and sleeper result in a random vibrating load. However, the unsprung mass and the space between the wheel and rail and the running speed are invariable. Thus, the train load can be simulated through the excitation function [22–25], for which the static load, irregularity, additional dynamic load, rail surface wave, and other random elements of trains under different frequencies will be taken into consideration, through the following expression:

$$F(t) = A_0 + A_1 \sin \omega_1 t + A_2 \sin \omega_2 t + A_3 \sin \omega_3 t, \quad (13)$$

where A_0 is the static load of wheel, and A_1, A_2, and A_3 refer to vibrating load, corresponding to typical values of control cases ①~③ in Table 4. With M_0 representing the unsprung mass, the amplitude of the corresponding vibrating load is

$$A_i = M_0 a_i \omega_i^2 \quad (i = 1, 2, 3), \quad (14)$$

where a_i is the typical vector height, corresponding to the three cases ①, ②, and ③ in Table 4; ω_i is the circular
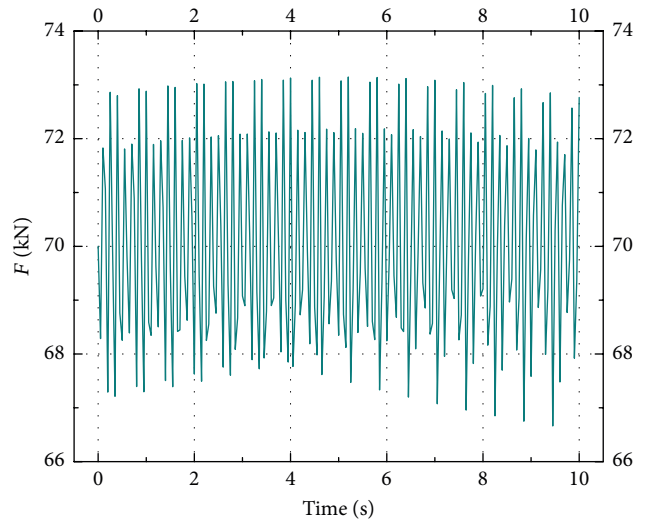
frequency of irregularity vibration wavelength under the corresponding vehicle speed, which in turn corresponds to the relevant cases ①, ②, and ③ in Table 4, with the following calculation:

$$\omega_i = \frac{2\pi v}{L_i} \quad (i = 1, 2, 3), \quad (15)$$

where v is the running speed of the train and L_i is the typical wavelength corresponding to the three cases ①, ②, and ③ in Table 4.

The trains for Xi'an Metro Line 2 are B-type, six-car metro trains, including three powered trains and three unpowered trains [26–29]. The unilateral static wheel load is 70 kN, and the unsprung mass is 750 kg. The irregular vibrating wavelength and vector height corresponding to three cases ①, ②, and ③ are as follows: $L_1 = 10$ m, $a_1 = 3.5$ mm; $L_2 = 2$ m, $a_2 = 0.4$ mm; $L_3 = 0.5$ m, $a_3 = 0.08$ mm, respectively. Figure 6 depicts the vibrating load versus time curve on the track subgrade in the first 10 s.

The most common physical quantity for measuring the influence on buildings is the vibration velocity. It can directly reflect the damage intensity of buildings and energy magnitude of structures for vibration response that is directly related to the destruction of these buildings, and thus it plays

TABLE 5: Calibration with measured and calculated velocities at different studied positions (unit: mm/s) [33].

Studied positions		A	B	C	D
Positive peak values	Registered velocities	0.4065	0.4786	0.6049	0.6793
	Calculated velocities	0.4403	0.5074	0.6253	0.6970
	Error (%)	8.31	6.02	3.37	2.61
Negative peak values	Registered velocities	−0.3926	−0.4712	−0.6070	−0.6989
	Calculated velocities	−0.4320	−0.5043	−0.6286	−0.7127
	Error (%)	10.04	7.02	3.56	1.97

a crucial role in the vibration of buildings [30, 31]. Under the independent action of metro train, the results calculated by numerical model are compared with real velocities measured in field tests to calibrate the model (Table 5). It can be seen that the real and calculated peak values (positive and negative) are very similar at the different studied positions. Consequently, it can be concluded that the numerical model developed is able to represent the dynamic behaviour of the studied tunnel.

5. Computation Result Analysis

To better study the vibration response of the Yongningmen tunnel operation on the metro line, two conditions of independent action of metro train (Condition 1) and the combined action of vehicles and train (Condition 2) were analyzed, and the response rules were obtained through the comparison of these two conditions. Under Condition 1, a metro train enters the simulation section with a running speed of 60 km/h at 0 s, with 12 s required for the train to completely pull out of the simulation section. To make the data more comprehensive, the data of 0 s–15 s are adopted for analysis. On the basis of the study of Condition 1, Condition 2 adopts the most dangerous moment of the section caused by vibration and makes vehicle load through the section to obtain the data in the dangerous condition. Therefore, the vehicle load enters the simulation section at 4.7 s and completely pulls out of the simulation section at 4.7 s with the running speed of 50 km/h. A cross section for every 2 m from the self-centred position towards one of the directions was adopted to account for the symmetrical structure, totalling 15 cross sections selected, as shown in Figure 7. The vibration response of the tunnel is obtained by analyzing the time history of acceleration, velocity, displacement, and Von Mises stress.

5.1. Vibration Response Analysis. The maximum and minimum values of each cross section at A, B, C, and D are shown in Figures 8–11. In Figure 8(a), the maximum value of acceleration increases from 1# cross section to 4# cross section and then gradually decreases and basically tends to be stable, whereas the opposite is true for the minimum value. Within the 1# and 7# cross sections, the difference of the same cross section under the two working conditions is apparent. After the 7# cross section, the two curves basically overlap, without any difference, indicating that the influence

of vehicle load reaches to 7# cross section, 14 m away from the centre. It provides the range of influence of vehicle load, which is beneficial to the shock absorption design of similar engineering. The trend of the variation curve (Figure 8(b)) for the velocity extremes with section location is the same as that of the acceleration, but under the two conditions, the maximum velocity curves basically overlap each other, and the difference is not significant; although the minimum velocity curves do not overlap each other, the difference is smaller, which indicates that vehicle load effect exerts less influence on speed compared to acceleration. In Figure 8(c), the various sections share the same maximum and minimum displacement values, so the curve trend is gentle. Moreover, the extreme values of displacement under the two conditions are similar, with the motor vehicle load effect and the maximum and minimum displacement values remaining constant.

It can be seen from the acceleration diagram in Figures 8–11 that with the moving down of the location of extraction point the curve shows certain volatility, dependent on the actual engineering structure. The difference between the two conditions also decreases with the moving down of the location of extraction point, along with the velocity curve, which signifies the declining influence on lining from A to B, C, and D with the motor vehicle load. So in the design and construction period we should take into account the vibration response of the vault and adopt some damping measures when necessary. Based on the velocity figures, it can be seen that various sections under two conditions have nearly the same maximum velocity, exerting the greatest influence on the extreme value of acceleration, followed by extreme value of velocity, and no influence on the extreme value of displacement. Therefore, in the process of vibration response analysis, it is unreasonable to use speed as an individual criterion, and the influence of acceleration should be taken into consideration. Moreover, according to the various figures, it can be found that the maximum value of the curve always appears at Section 4# or 5#, and the extreme value at point A is the minimum, while the extreme value at point D is the maximum. Therefore, the time-history curve at point D at the two sections under Condition 2 is selected for analysis (see Figure 12).

5.2. Time-History Response Analysis. Figure 12 indicates that the time-history curve has five periods, with various periods
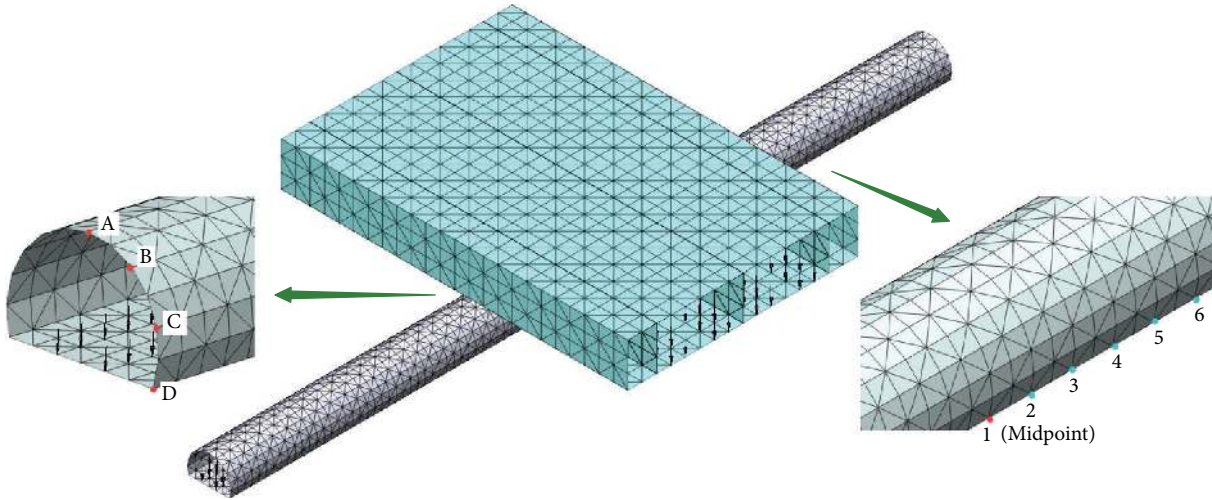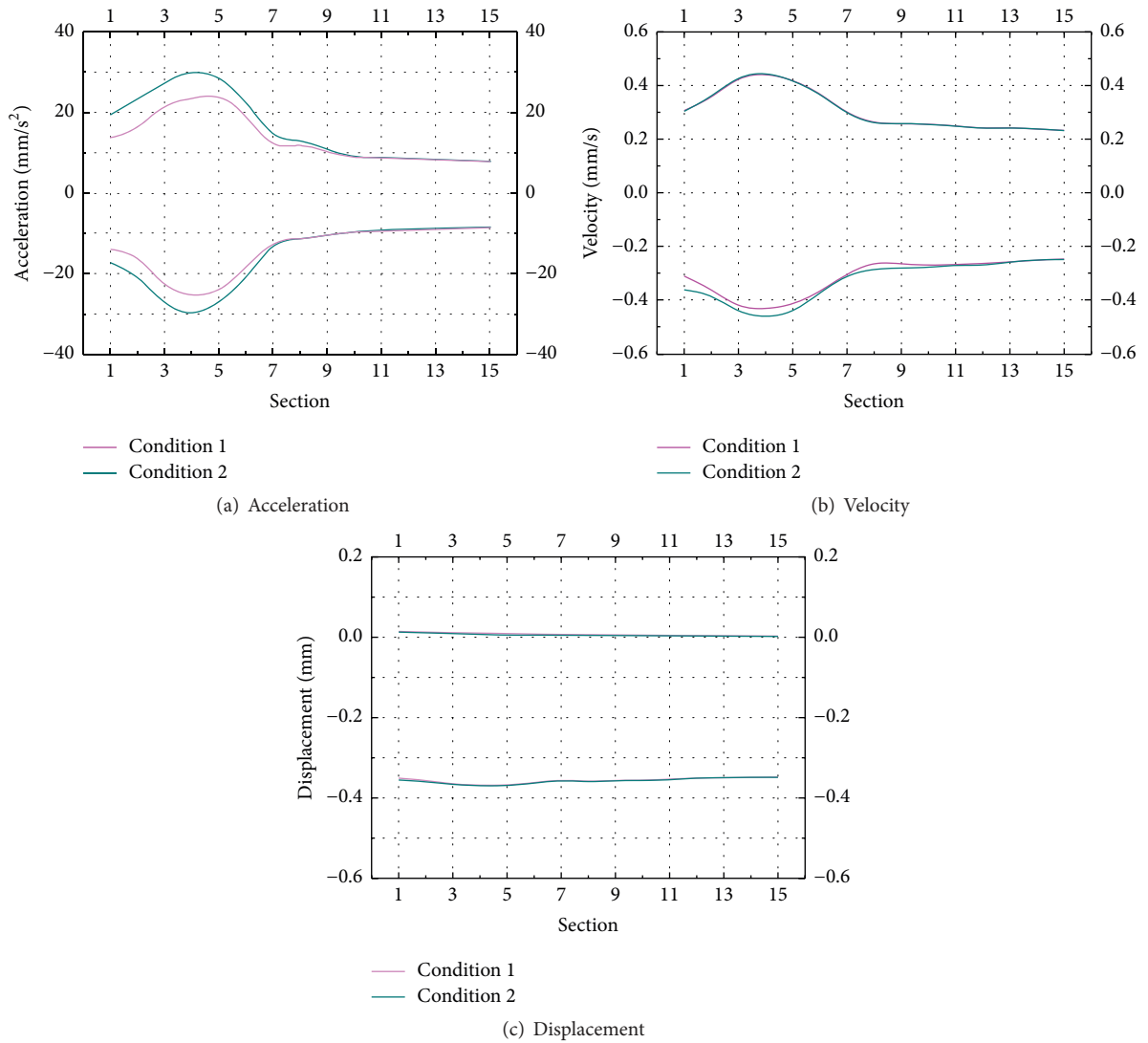
FIGURE 7: Location of selected points.

(a) Acceleration

(b) Velocity

(c) Displacement

FIGURE 8: The maximum and minimum values of point A in two conditions: (a) acceleration, (b) velocity, and (c) displacement.

(a) Acceleration
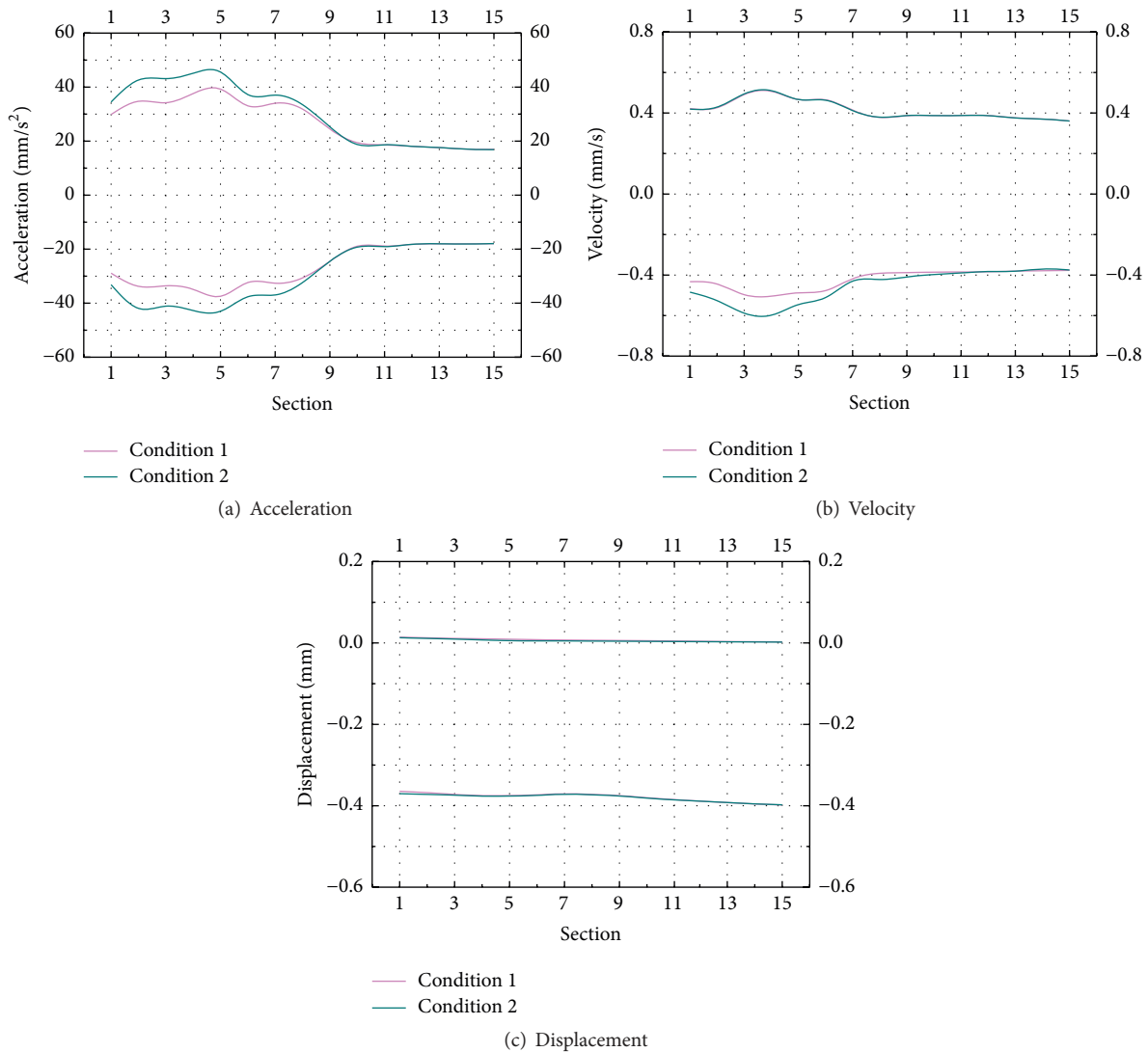
(b) Velocity

(c) Displacement

FIGURE 9: The maximum and minimum values of point B in two conditions: (a) acceleration, (b) velocity, and (c) displacement.

corresponding to the running position of the train (Figure 13); assuming the length of the train is l and taking the position of study as the original point and running direction of the train as the positive direction, the following analysis was conducted.

(1) Close Period. Within the period when the train drives into the simulation section and has run for 2 s, the location of the locomotive corresponding to the study point is $[-\infty, -25]$. During this period, the numerical value of acceleration approaches 0, with smaller variation. Although some variation is present within the velocity curve, its numerical value is small; the displacement value has variation nearby value 0, but in terms of general trend it increases gradually towards the negative direction.

(2) Rising Period. When the train has run for 2 s to 4 s, the location of the locomotive corresponding to the study point is $[-25, 8]$. The fluctuation amplitude of acceleration rises

rapidly from 2 s, reaching its maximum at 3 s, and then gradually decreases from 3 s to 4 s. The fluctuation amplitude of the velocity curve increases sharply, but the overall value tends towards the negative direction; the displacement value rises sharply during this period, with the acceleration and velocity reaching maxima, namely, $-99.30 \, \text{mm/s}^2$ (Section 5#) and $-0.71 \, \text{mm/s}$ (Section 4#), respectively. This is less than the standard value of structure safety vibration control, thus maintaining a safety status.

(3) Stable Period. When the train has run for 4 s to 7 s, the location of the locomotive corresponding to the study point is $[8, l - 33]$. During this period, the acceleration and velocity curve form a relative stable status with continuous fluctuation; however, the displacement reaches the maximum during this period and has certain fluctuations near the maximum. During this period, the displacement value reaches the maximum value, namely, $-0.40 \, \text{mm}$. This is less than

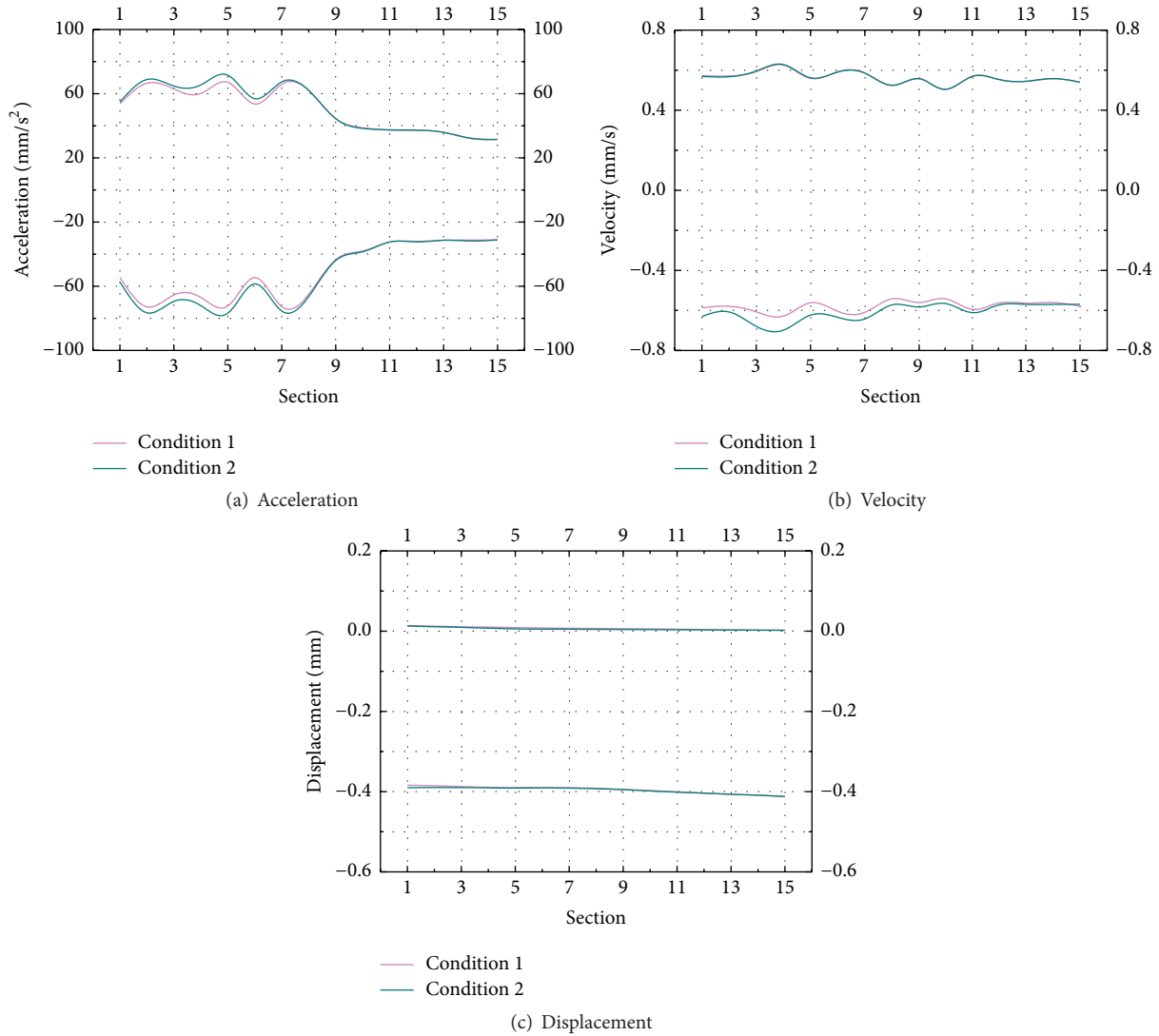(a) Acceleration

(b) Velocity

(c) Displacement

FIGURE 10: The maximum and minimum values of point C in two conditions: (a) acceleration, (b) velocity, and (c) displacement.

the standard value of structure safety vibration control, thus maintaining a safety status.

(4) Declining Period. When the train has run for 7 s to 9 s, the location of locomotive corresponding to the study point is $[l - 33, l - 8]$. Similar to the second period, the fluctuation amplitude of acceleration and speed rises sharply from 7 s, and the peak acceleration appears near 8 s, although it is less than the peak value in the second period due to the motor vehicle load. The overall value of velocity tends towards the positive direction; the displacement value during this period decreases greatly and tends to be 0.

(5) Leaving Period. After 9 s, the location of the locomotive corresponding to the study point is $[l - 8, +\infty]$, and as time goes by, the variation amplitude of acceleration, velocity, and displacement are gradually reduced, with the value tending to be 0.

According to the above analysis, within the rising period, stable period, and declining period, the original point will be the existence of vibration response. And the acceleration and velocity should be used as criteria for the evaluation of vibration in rising period and declining period, while the displacement is used as criteria in stable period.

5.3. Mechanical Response Analysis. Figure 14 is the lining Von Mises stress under two conditions. After comparison it was found that the stress of the tunnel lining near Yongningmen tunnel is improved due to the motor vehicle load. However, the maximum stress value of the lining increased to 204.77 kPa from 197.56 kPa, with small rising amplitude and the lining remaining within the safety range. Typical sections such as 4# and 5# were selected for analysis under two conditions. Because of bilateral symmetry, 50% of the data is selected to draw the Von Mises stress envelope curve,

TABLE 6: Verification with measured and calculated velocities at different studied positions (unit: mm/s) [33].

Studied positions		A	B	C	D
	Measured velocities	0.4498	0.5231	0.6355	0.7075
Positive peak values	Calculated velocities	0.4434	0.5105	0.6284	0.7000
	Error (%)	1.42	2.41	1.12	1.06
	Measured velocities	−0.4527	−0.5589	−0.6648	−0.7452
Negative peak values	Calculated velocities	−0.4609	−0.5982	−0.6989	−0.7621
	Error (%)	1.81	7.03	5.13	2.27

(a) Acceleration

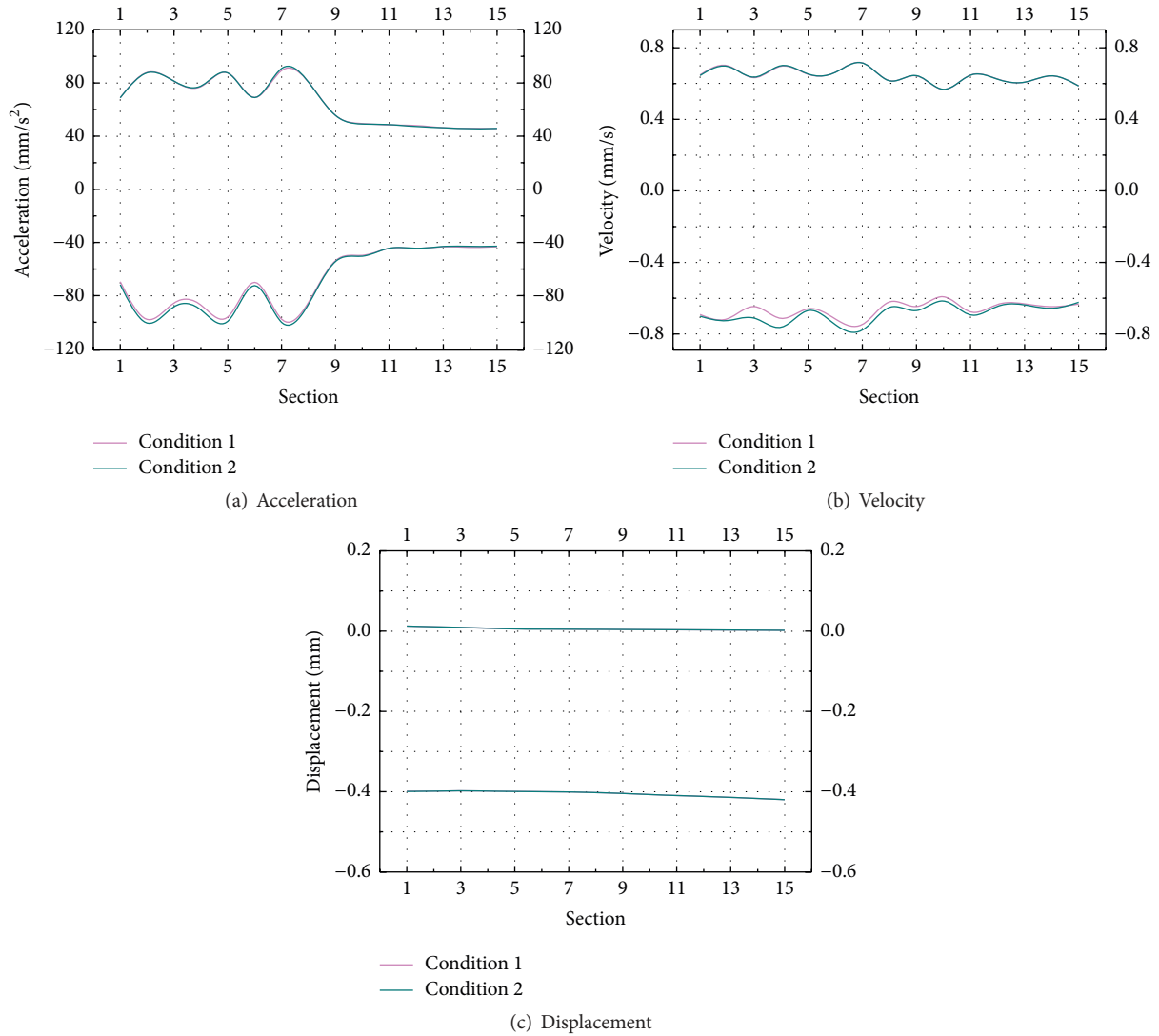
(b) Velocity

(c) Displacement

FIGURE 11: The maximum and minimum values of point D in two conditions: (a) acceleration, (b) velocity, and (c) displacement.

as shown in Figure 15. It can be seen from the figure that the stress value at different positions under Condition 2 has been significantly improved compared to that under Condition 1, but the relative magnitudes at different positions still remain the same, gradually increasing from point 1 to point 6 and decreasing at point 7. This result implies that point 6 becomes the most dangerous and vulnerable position, the stress of which should be focused and strictly controlled.

5.4. Demonstration of Numerical Modelling. To validate the model, calculation results were compared with those of field tests under Condition 2 when the train velocity is 60 km/h (Table 6). According to the above analysis, the four points (A, B, C, and D) are key and thus monitored (Figure 16). It can be observed that the difference for peak values (positive and negative) is not significant between measured and calculated velocities. Moreover, these maximums and minimums occur

(a) Acceleration
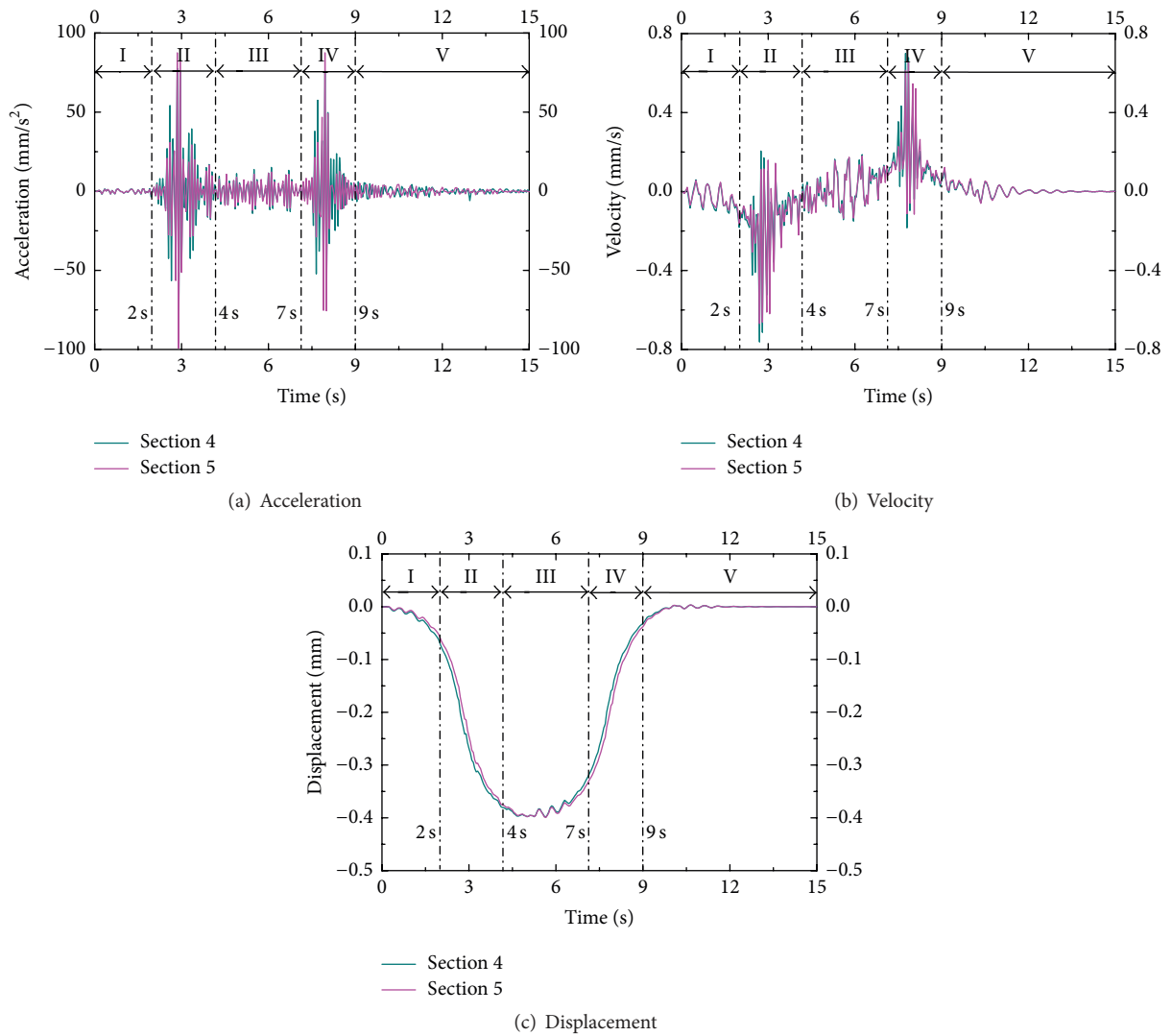

(b) Velocity

(c) Displacement

Figure 12: Time history of the (a) acceleration, (b) velocity, and (c) displacement at point D.
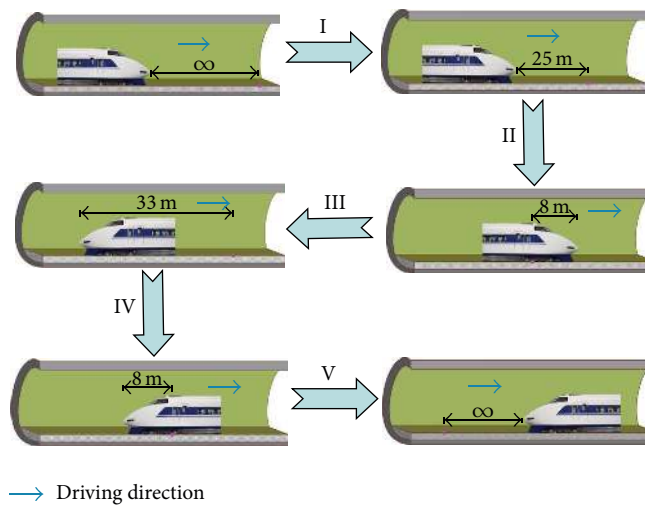
Figure 13: Various periods corresponding to the running position of the train.

2D element stress
Von Mises stress
unit (kN/m^2)

0.2%	$+1.97561e + 002$
0.6%	$+1.85660e + 002$
1.6%	$+1.73760e + 002$
3.7%	$+1.61859e + 002$
5.8%	$+1.49959e + 002$
7.1%	$+1.38058e + 002$
7.8%	$+1.26158e + 002$
7.1%	$+1.14257e + 002$
7.6%	$+1.02357e + 002$
8.5%	$+9.04565e + 001$
8.0%	$+7.85561e + 001$
7.9%	$+6.66556e + 001$
9.1%	$+5.47552e + 001$
12.9%	$+4.28547e + 001$
10.9%	$+3.09543e + 001$
1.2%	$+1.90538e + 001$
	$+7.15334e + 000$

(a) Condition 1

2D element stress
Von Mises stress
unit (kN/m^2)

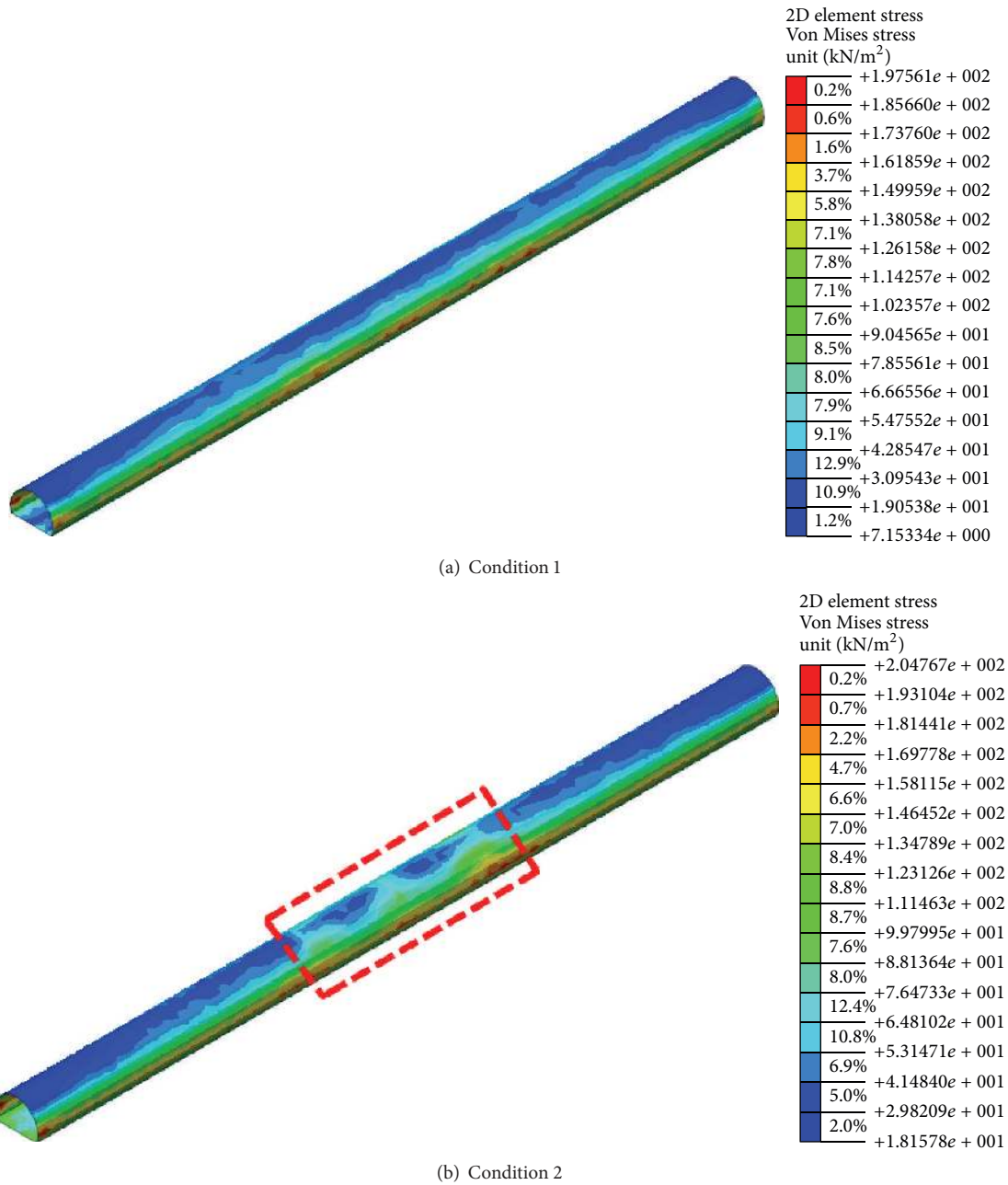|	
0.2%	$+2.04767e + 002$
0.7%	$+1.93104e + 002$
2.2%	$+1.81441e + 002$
4.7%	$+1.69778e + 002$
6.6%	$+1.58115e + 002$
7.0%	$+1.46452e + 002$
8.4%	$+1.34789e + 002$
8.8%	$+1.23126e + 002$
8.7%	$+1.11463e + 002$
7.6%	$+9.97995e + 001$
8.0%	$+8.81364e + 001$
12.4%	$+7.64733e + 001$
10.8%	$+6.48102e + 001$
6.9%	$+5.31471e + 001$
5.0%	$+4.14840e + 001$
2.0%	$+2.98209e + 001$
	$+1.81578e + 001$

(b) Condition 2

Figure 14: Von Mises stress (unit: kPa).

at the same time in the time-history curves, which show the overlapping of a real velocity register and the obtained from the numerical model. The velocities of four points are consistent with field data, which indicate that the model in this paper can quantitatively reflect the actual vibration response of structure.

6. Concluding Remarks

Vibration response induced by tunnel vehicle load and metro train load to the structure of shield tunnel was analyzed by applying 3D dynamic finite element model in this study.

Through the above case analysis and results, we can obtain the following conclusions and perspectives.

(1) The numerical simulation results were validated by the data registers measured in field tests. The results show that the modelling procedure is consistent with the actual situation and can be used to predict the vibration response of a similar underground structure.

(2) The motor vehicle load only affects the metro tunnel within 14 m from the centre, and the influence decreases progressively from vault to spandrel,
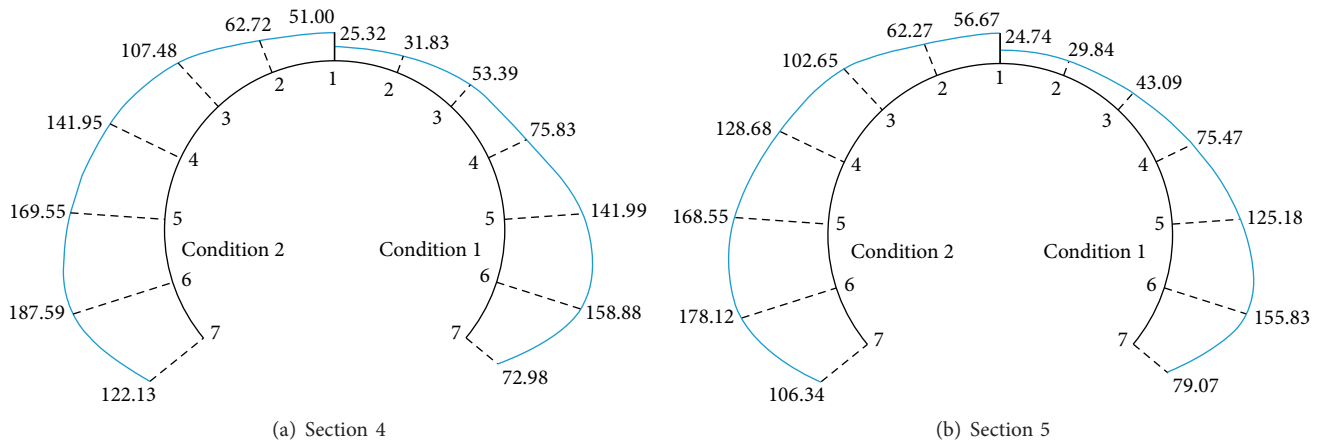
(a) Section 4

(b) Section 5

FIGURE 15: Von Mises stress envelope curve (unit: kPa).

FIGURE 16: On-site monitoring [33].

haunch, and springing. So, in the process of engineering design, attention should be paid to the vibration response of the vault within this range and it should be conducted by taking some damping measures when necessary.

(3) The running train has five periods for vibration response, namely, close period, rising period, stable period, declining period, and leaving period. The location of the locomotive corresponding to the study point in these periods is $[-\infty, -25]$, $[-25, 8]$, $[8, l - 33]$, $[l - 33, l - 8]$, and $[l - 8, +\infty]$, respectively. The original point will be the existence of vibration response only in the middle three stages, which is conducive to the range choice of research time and space, and provides a theoretical basis for the development of various periods of the evaluation criteria.

(4) Due to vehicle load, the stress of the metro tunnel lining near Yongningmen tunnel has been improved substantially increasing from vault to haunch and decreasing slightly at springing. Therefore, the stress value at haunch should be considered carefully.

(5) With the increasing of the tunnel and subway systems around the world, specifically the Northwest of China, such as Lanzhou, Xi'an, and Taiyuan, there will be a lot of cross tunnel structures. The vibration response cannot be ignored because the train vibration will bring serious impact to the existing engineering structure, especially the ancient buildings. Moreover, since the formation is similar in that region, loess has a wide distribution, and the conclusions of this paper will have a certain reference value for further research and practical application in the Northwest of China.

(6) Numerous studies utilizing dynamic finite element method to solve the vibration problem, the field observation datasets, and numerical simulation results were compared, but we only concentrated on acceleration, velocity, and displacement. We can strengthen the research results in the stress response and then study the relationship between vibration peak velocity and stress, making a complete system to evaluate the effect of structural vibration.

Competing Interests

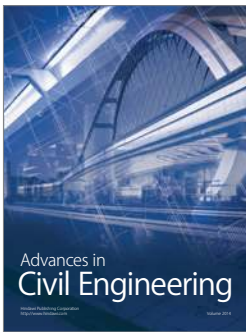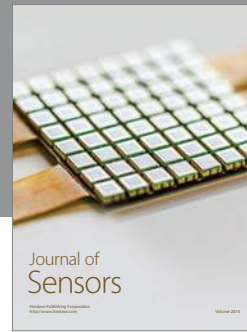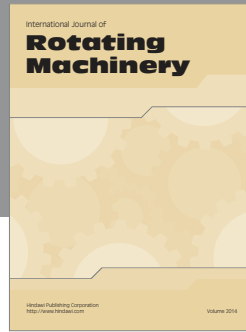The authors declare that there are no competing interests regarding the publication of this paper.

Acknowledgments

References

[1] T. Balendra, C. G. Koh, and Y. C. Ho, "Dynamic response of buildings due to trains in underground tunnels," *Earthquake Engineering and Structural Dynamics*, vol. 20, no. 3, pp. 275–291, 1991.

[2] E. Soliman, H. Duddeck, and H. Ahrens, "Two- and three-dimensional analysis of closely spaced double-tube tunnels," *Tunnelling and Underground Space Technology incorporating Trenchless*, vol. 8, no. 1, pp. 13–18, 1993.

[3] I. Yamaguchi, I. Yamazaki, and Y. Kiritani, "Study of ground-tunnel interactions of four shield tunnels driven in close proximity, in relation to design and construction of parallel shield tunnels," *Tunnelling and Underground Space Technology*, vol. 13, no. 3, pp. 289–304, 1998.

[4] P. Koziol and C. Mares, "Wavelet approach for vibration analysis of fast moving load on a viscoelastic medium," *Shock and Vibration*, vol. 17, no. 4-5, pp. 461–472, 2010.

[5] W. B. Shi, L. C. Miao, Z. X. Wang, and J. H. Luo, "Settlement behaviors of metro tunnels during the metro operation," *Shock and Vibration*, vol. 2015, Article ID 863961, 11 pages, 2015.

[6] H. Zhong, D. Qu, G. Lin, and H. Li, "Application of sensor networks to the measurement of subway-induced ground-borne vibration near the station," *International Journal of Distributed Sensor Networks*, vol. 2014, Article ID 181453, 10 pages, 2014.

[7] J. X. Lai, H. B. Fan, J. X. Chen, J. L. Qiu, and K. Wang, "Blasting vibration monitoring of undercrossing railway tunnel using wireless sensor network," *International Journal of Distributed Sensor Networks*, vol. 2015, Article ID 703980, 7 pages, 2015.

[8] Z. P. Liao, *Introduction to Wave Motion Theories in Engineering*, Science Press, Beijing, China, 2002.

[9] MIDAS Information Technology Co, *Midas GTS User Manual*, MIDAS Information Technology Co., Beijing, China, 2005.

[10] M. Ma, W. N. Liu, C. Y. Qian, G. H. Deng, and Y. D. Li, "Study of the train-induced vibration impact on a historic Bell Tower above two spatially overlapping metro lines," *Soil Dynamics and Earthquake Engineering*, vol. 81, pp. 58–74, 2016.

[11] H. R. Nejati, M. Ahmadi, and H. Hashemolhosseini, "Numerical analysis of ground surface vibration induced by underground train movement," *Tunnelling and Underground Space Technology*, vol. 29, pp. 1–9, 2012.

[12] J. X. Lai, C. X. Guo, J. L. Qiu, and H. B. Fan, "Static analytical approach of moderately thick cylindrical ribbed shells based on first-order shear deformation theory," *Mathematical Problems in Engineering*, vol. 2015, Article ID 274091, 14 pages, 2015.

[13] Y. Chun-Shan, M. Hai-Hong, C. Jun-Sheng, and W. Yi-Zhao, "Influence of seismic loading on segment opening of a shield tunnel," *The Scientific World Journal*, vol. 2014, Article ID 387210, 9 pages, 2014.

[14] A. Yaseri, M. H. Bazyar, and N. Hataf, "3D coupled scaled boundary finite-element/finite-element analysis of ground vibrations induced by underground train movement," *Computers and Geotechnics*, vol. 60, pp. 1–8, 2014.

[15] W. White, S. Valliappan, and I. K. Lee, "Unified boundary for finite dynamic models," *Journal of the Engineering Mechanics Division*, vol. 103, no. 5, pp. 949–964, 1977.

[16] Q. S. Zhang, "Dynamic analysis and experiments of car driving on uneven road," *Journal of Central South Highway Engineering*, vol. 2, pp. 116–128, 1983.

[17] J. X. Lai, J. L. Qiu, J. X. Chen, H. B. Fan, and K. Wang, "New technology and experimental study on snow-melting heated pavement system in tunnel portal," *Advances in Materials Science and Engineering*, vol. 2015, Article ID 706536, 11 pages, 2015.

[18] S. Gupta, W. F. Liu, G. Degrande, G. Lombaert, and W. N. Liu, "Prediction of vibrations induced by underground railway traffic in Beijing," *Journal of Sound and Vibration*, vol. 310, no. 3, pp. 608–630, 2008.

[19] S. Gupta, H. Van den Berghe, G. Lombaert, and G. Degrande, "Numerical modelling of vibrations from a Thalys high speed train in the Groene Hart tunnel," *Soil Dynamics and Earthquake Engineering*, vol. 30, no. 3, pp. 82–97, 2010.

[20] H. P. Lai, S. Guo, and Y. L. Xie, "Assessment of fire-induced damage and restoration programme in Xinqidaoliang road tunnel," *Magazine of Concrete Research*, vol. 66, no. 13, pp. 652–660, 2014.

[21] J. O'Brien and D. C. Rizos, "A 3D BEM-FEM methodology for simulation of high speed train induced vibrations," *Soil Dynamics and Earthquake Engineering*, vol. 25, no. 4, pp. 289–301, 2005.

[22] L. Li, B. Q. Zhang, and X. L. Yang, "Analysis of dynamic response of large cross-section tunnel under vibrating load induced by high speed train," *Chinese Journal of Rock Mechanics and Engineering*, vol. 24, no. 23, pp. 4259–4265, 2005.

[23] F. Ye, C. He, S. M. Wang, and J. L. Zhang, "Landscape design of mountain highway tunnel portals in China," *Tunnelling and Underground Space Technology*, vol. 29, pp. 52–68, 2012.

[24] C. S. Yang, H. H. Mo, J. S. Chen, and J. Wang, "Numerical analysis of influences caused by lining cracks on dynamic response of shield tunnel during metro operation," *Journal of Information and Computational Science*, vol. 11, no. 11, pp. 3835–3846, 2014.

[25] J. X. Lai, S. Mao, J. L. Qiu et al., "Investigation progresses and applications of fractional derivative model in geotechnical engineering," *Mathematical Problems in Engineering*, vol. 2016, Article ID 9183296, 15 pages, 2016.

[26] J.-B. Zhou, H. Chen, J. Yang, and J. Yan, "Pedestrian evacuation time model for urban metro hubs based on multiple video sequences data," *Mathematical Problems in Engineering*, vol. 2014, Article ID 843096, 11 pages, 2014.

[27] Y. Q. Wang, L. Li, Z. C. Wang, T. Lv, and L. Wang, "Mode shift behavior impacts from the introduction of metro service: case study of Xi'an, China," *Journal of Urban Planning and Development*, vol. 139, no. 3, pp. 216–225, 2013.

[28] F. Ye, C. F. Gou, H. D. Sun, Y. P. Liu, Y. X. Xia, and Z. Zhou, "Model test study on effective ratio of segment transverse bending rigidity of shield tunnel," *Tunnelling and Underground Space Technology*, vol. 41, no. 1, pp. 193–205, 2014.

[29] J. Lai, J. Qiu, H. Fan et al., "Fiber bragg grating sensors-based in-situ monitoring and safety assessment of loess tunnel," *Journal of Sensors*, In press.

[30] H. T. Yu, J. T. Chen, A. Bobet, and Y. Yong, "Damage observation and assessment of the Longxi tunnel during the Wenchuan earthquake," *Tunnelling and Underground Space Technology*, vol. 54, pp. 102–116, 2016.

[31] H. B. Zhao, Y. Long, X. H. Li, and L. Lu, "Experimental and numerical investigation of the effect of blast-induced vibration from adjacent tunnel on existing tunnel," *KSCE Journal of Civil Engineering*, vol. 20, no. 1, pp. 431–439, 2016.

[32] Shaanxi Institute of Engineering Prospecting, *Geotechnical Investigation Report of Metro Line 2 between Yongningmen and the Bell Tower*, Shaanxi Institute of Engineering Prospecting, Xi'an, China, 2004.

[33] S. B. Zhang, *Dynamic Response Test Report between Metro Line 2 and Yongningmen Tunnel in Xi'an*, Xi'an Metro Co., Xi'an, China, 2014.